

# Phase Transitions in Pores: Experimental and Simulation Studies of Melting and Freezing<sup>†</sup>

Malgorzata Sliwinska-Bartkowiak, Jolanta Gras, and Roman Sikorski

Instytut Fizyki, Uniwersytet im Adama Mickiewicza, ul. Grunwaldzka, 60-780 Poznan, Poland

Ravi Radhakrishnan, Lev Gelb, and Keith E. Gubbins\*

Department of Chemical Engineering, 113 Riddick Labs, North Carolina State University, Raleigh, North Carolina 27695-7905

Received October 19, 1998. In Final Form: February 3, 1999

We report both experimental measurements and molecular simulations of the melting and freezing behavior of simple fluids in porous media. The experimental studies are for carbon tetrachloride and nitrobenzene in controlled pore glass (CPG) and Vycor. Differential scanning calorimetry (DSC) was used to determine the melting point in the porous materials for each of the glass samples. In the case of nitrobenzene (which has a nonzero dipole moment), dielectric spectroscopy was also used to determine melting points. Measurements by the two methods were in excellent agreement. The melting point was found to be depressed relative to the bulk value for both fluids. With the exception of smallest pores, the melting point depression was proportional to the reciprocal of the pore diameter, in agreement with the Gibbs–Thomson equation. Structural information about the different confined phases was obtained by measuring the dielectric relaxation times using dielectric spectroscopy. Monte Carlo simulations were used to determine the shift in the melting point,  $T_m$ , for a simple fluid in pores having both repulsive and strongly attractive walls. The strength of attraction to the wall was shown to have a large effect on the shift in  $T_m$ , with  $T_m$  being reduced for weakly attracting walls. For strongly attracting walls, such as graphitic carbon, the melting point increases for slit-shaped pores. For such materials, the adsorbed contact layer is shown to melt at a higher temperature than the inner adsorbed layers. A method for calculating the free energies of solids in pores is presented, and it is shown that the solid–liquid transition is first order in these systems.

## 1. Introduction

There has been growing interest in the study of fluid–solid transitions in porous materials. Important questions regarding melting and freezing in pores are the nature of the phase transition (first order vs continuous), the direction of shift in the melting temperature  $T_m$ , the nature and origin of hysteresis, the dimensionality crossover due to increasing confinement, the structural changes of the condensed phases in the restricted pore geometries, the effect on latent heats, etc. Improved understanding of confinement effects on freezing are essential in areas relating to lubrication, adhesion, fabrication of nano-materials, and nanotribology. In addition, these studies can provide insight into mechanisms involved in frost heaving and distribution of pollutants in soil. Freezing in porous media has also been widely employed in the characterization of porous materials using the method of thermoporometry.<sup>1</sup>

There have been several experimental studies of melting and freezing in well-characterized porous materials. Most experiments have used porous silica glasses as the confinement media and found a decrease in freezing point of the confined fluid as compared to the bulk.<sup>2–15</sup> Such

glasses have a complex networked structure of roughly cylindrical pores and have a narrow size distribution about a mean radius. In all of these studies, the lowering of the melting temperature increases as the pore width  $H$  decreases and, for larger pores, is roughly proportional to  $H^{-1}$  as predicted by the Gibbs–Thomson equation<sup>16</sup>

$$\frac{T_{m,\text{bulk}} - T_{m,\text{pore}}}{T_{m,\text{bulk}}} = 2 \frac{(\gamma_{\text{ws}} - \gamma_{\text{wl}})V}{H\lambda_{m,\text{bulk}}} \quad (1)$$

where  $T_{m,\text{bulk}}$  and  $T_{m,\text{pore}}$  are the melting temperatures of the bulk sample and the confined sample, respectively,

\* Corresponding author. Tel: 919-513-2262. Fax: 919-515-3465. E-mail: keg@ncsu.edu.

<sup>†</sup> Presented at the Third International Symposium on Effects of Surface Heterogeneity in Adsorption and Catalysis on Solids, held in Poland, August 9–16, 1998.

(1) Eyraud, C.; Quinson, J. F.; Brun, M. *Characterization of Porous Solids*; Unger, K., Rouquerol, J., Sing, K. S. W., Kral, H., Eds.; Elsevier: Amsterdam, 1988; p 307.

(2) Warnock, J.; Awaschalom, D. D.; Shafer, M. W. *Phys. Rev. Lett.* 1986, 57, 1753.

(3) Tell, J. L.; Maris, H. J.; Seidel, G. M. *Phys. Rev. B* 1983, 28, 5122.

(4) Torii, R. H.; Maris, H. J.; Seidel, G. M. *Phys. Rev. B* 1990, 41, 7167.

(5) Sokol, P. E.; Ma, W. J.; Herwig, K. E.; Snow, W. M.; Wang, Y.; Koplik, J.; Banavar, J. R. *Appl. Phys. Lett.* 1992, 61, 777.

(6) Strange, J. H.; Rahman, M.; Smith, E. G. *Phys. Rev. Lett.* 1993, 71, 3589.

(7) Molz, E.; Wong, A. P. Y.; Chan, M. H. W.; Beamish, J. R. *Phys. Rev. B* 1993, 48, 5741.

(8) Unruh, K. M.; Huber, T. E.; Huber, C. A. *Phys. Rev. B* 1993, 48, 9021.

(9) Duffy, J. A.; Wilkinson, N. J.; Fretwell, H. M.; Alam, M. A.; Evans, R. J. *Phys. Condens. Matter* 1995, 7, L713.

(10) Hansen, E. W.; Stöker, M.; Schmidt, R. J. *Phys. Chem.* 1996, 100, 2195.

(11) Elder, K. J.; Reynolds, P. A.; Trouw, F.; White, J. W. J. *Chem. Soc., Chem. Commun.* 1996, 155.

(12) Krim, J.; Coulomb, J. P.; Bouzidi, J. *Phys. Rev. Lett.* 1987, 58, 583.

(13) Morishige, K.; Nobuoka, K. J. *Chem. Phys.* 1997, 107, 6965.

(14) Overloop, K.; Van Gerven, L. J. *Magn. Reson., Ser. A* 1993, 101, 179.

(15) Booth, H. F.; Strange, J. H. *Mol. Phys.* 1998, 93, 263.

(16) Evans, R.; Marconi, U. M. B. *J. Chem. Phys.* 1987, 86, 7138.

$\gamma_{ws}$  and  $\gamma_{wl}$  are the corresponding wall–solid and wall–fluid surface tensions,  $v$  is the molar volume of the bulk liquid, and  $\lambda_{m,bulk}$  is the latent heat of melting in the bulk.

An opposing trend in the freezing point shift was reported by Klein and Kumacheva.<sup>17</sup> These authors studied freezing of cyclohexane between parallel mica surfaces (slit-shaped geometry) and observed a significant increase of about 17 K in the melting temperature on confinement for a 4.0 nm pore. Such an increase is consistent with the Gibbs–Thomson equation if one recognizes that the direction of the freezing point shift depends on whether the pore wall favors the confined solid phase or the confined fluid phase. If the wall–solid surface tension,  $\gamma_{ws}$ , is greater than the wall–fluid surface tension,  $\gamma_{wl}$ , then the shift  $\Delta T_m = T_{m,bulk} - T_{m,pore}$  is predicted to be positive; otherwise, it is negative. Some of the studies<sup>7,8</sup> also reported latent heat measurements in the confined systems, and these were less than the bulk values. There have been some experimental reports that investigated the structure of the confined phases using NMR and X-ray diffraction techniques.<sup>13–15</sup> These studies involved different fluids in silica-based pores in which the freezing temperature was always depressed, and suggested that the contact layer (the layer adjacent to the pore walls, about 2–3 molecular diameters wide) melts at a lower temperature than the interior of the pore, in the confined solid phase.

Molecular simulation studies<sup>18–20</sup> were recently carried out in an attempt to explain the differences in the freezing point behavior. Miyahara and Gubbins<sup>18</sup> studied the freezing of Lennard–Jones methane in slit-shaped pores with different pore–wall interactions. They concluded that the shift in freezing temperature,  $\Delta T_f = T_{f,bulk} - T_{f,pore}$ , was negative if the fluid–wall interaction is more strongly attractive than the fluid–fluid interaction and positive if the fluid–wall interaction was less attractive than the fluid–fluid interaction. Maddox and Gubbins<sup>19</sup> studied freezing and melting of simple fluids in pores of cylindrical geometry and reached similar conclusions. However, they found important differences because of the increased confinement in a cylindrical geometry. In particular, the additional confinement led to downward shifts in the freezing temperatures when compared to confinement in a slit geometry. However, a limitation of these two simulation studies was that the precise location of the phase transition was not found. The freezing and melting displayed large hysteresis loops in the average density of the fluid adsorbed as a function of temperature, and thus the location of the equilibrium freezing/melting point could be estimated only to the accuracy of the width of the hysteresis loops. The nature of the transition was also not clear from the adsorption behavior. For slit pores with weakly attractive walls, Dominguez et al.<sup>20</sup> were able to use thermodynamic integration to evaluate the free energy of the confined phases. They were thus able to show that the freezing transition was first order and to locate the true equilibrium melting point. However, their method failed for more strongly attractive walls, due to freezing of the adsorbed contact layer adjacent to the wall.

In this paper, we study the melting of  $\text{CCl}_4$  and nitrobenzene in porous silica glasses of different mean pore diameters using differential scanning calorimetry (DSC) and dielectric spectroscopy (DS). We also describe a method that determines the true thermodynamic melting/freezing point of a fluid confined in a pore, using

a novel molecular simulation method to calculate the free energy of the condensed phases. This method is applied to freezing of Lennard–Jones methane in two different slit-shaped pores, having repulsive as well as strongly attractive walls. The rest of the paper is organized as follows. In section 2, we describe the experimental and simulation methods. We present our results in sections 3 and 4, followed by discussion and conclusions in section 5.

## 2. Methods

The DSC and DS experiments were performed at the A. Mickiewicz University, Poznan, Poland. The  $\text{CCl}_4$  and nitrobenzene samples were reagent grade chemicals and were twice distilled (nitrobenzene at reduced pressure) prior to use in the experiments. Nitrobenzene was further dried over  $\text{Al}_2\text{O}_3$ , centrifuged, and stored in the absence of light to avoid contamination by photochemical reactions. The conductivities of the purified  $\text{CCl}_4$  and nitrobenzene samples were found to be less than  $10^{-16}$  and  $10^{-10} \text{ } \Omega^{-1} \text{ m}^{-1}$ , respectively. The porous silica samples used were the commercially available Controlled Pore Glass (CPG) from CPG Inc., with a pore size distribution of about 5% around the mean pore diameter. Different CPG samples having average pore diameters ranging from 50 to 7.5 nm were used. We have also studied confinement in a Vycor glass from Corning Inc., having a mean pore size of 4.0 nm. The pore samples were kept under vacuum prior to and during the introduction of the fluid. The computer simulation studies were performed at the Cornell Theory Center using the IBM-SP2 supercomputer.

**2.1. Differential Scanning Calorimetry.** A Perkin–Elmer DSC7 (differential scanning calorimeter) was used to determine the melting temperatures and latent heats of fusion, by measuring the heat released in the melting of nitrobenzene. A Dupont thermal analyzer was used for the measurements involving  $\text{CCl}_4$ . The temperature scales of the two DSC machines were calibrated to the melting temperatures of pure nitrobenzene and  $\text{CCl}_4$ , respectively. The background of each raw DSC spectrum was subtracted, on the basis of a second-order polynomial fit to the measured heat flow, away from the signals of interest. The melting temperatures were determined from the positions of the peaks of the heat flow signals, and the latent heats were determined from the scaled areas under these signals. The melting temperatures were reproducible to within 0.5 °C for larger pores ( $\geq 25$  nm); uncertainties were larger for the smaller pores. These uncertainties are a result of the width of the DSC peaks, which derives in part from variations in pore size, and geometry, and from the existence of metastable states. The latent heats were reproducible to within an accuracy of 5%.

**2.2. Dielectric Spectroscopy.** The permittivity of a medium,  $\epsilon^* = \epsilon' - i\epsilon''$ , is in general a complex quantity whose real part  $\epsilon'$  is associated with the increase in capacitance due to the introduction of the dielectric. The imaginary component  $\epsilon''$  is associated with mechanisms that contribute to energy dissipation in the system; these include small but nonzero conductivity of the dielectric and viscous damping of the rotational motion of the dipolar molecules in alternating fields. The latter effect is frequency dependent. The relative permittivity  $\kappa^*$  is given by the ratio of the permittivity of the medium to that of free space:

$$\kappa^* = \kappa' - i\kappa'' = \epsilon^*/\epsilon_0 \quad (2)$$

The real part of the relative permittivity,  $\kappa' = \epsilon'/\epsilon_0$ , is also known as the dielectric constant. The experimental setup consisted of a parallel plate capacitor of empty capacitance  $C_0 = 4.2$  pF. The temperature was controlled to an accuracy of 0.1 °C by a Pt(100) platinum resistor using an external K30 Modingen cryostat. The capacitance,  $C$ , and the tangent loss,  $\tan(\delta)$ , of the capacitor filled with nitrobenzene between the plates were measured using a Solartron 1260 gain impedance analyzer, in the frequency range 1 Hz–10 MHz, for various temperatures.<sup>21</sup> For a given capacitor,

(17) Klein, J.; Kumacheva, E. *Science* 1995, 269, 816.

(18) Miyahara, M.; Gubbins, K. E. *J. Chem. Phys.* 1997, 106, 2865.

(19) Maddox, M.; Gubbins, K. E. *J. Chem. Phys.* 1997, 107, 9659.

(20) Dominguez, H.; Allen, M. P.; Evans, R. *Mol. Phys.* 1999, 96, 209.

(21) Chelkowski, A. *Dielectric Physics*; Elsevier/North-Holland, Inc.: New York, 1980.

the capacitance,  $C$ , is proportional to  $\epsilon'$ , the permittivity of the dielectric medium between the capacitor plates. The relative permittivity of nitrobenzene as a function of temperature was calculated using

$$\kappa' = C/C_0; \quad \kappa'' = \tan(\delta)/\kappa' \quad (3)$$

For the case of nitrobenzene in porous silica, the sample was introduced between the capacitor plates as a suspension of 200  $\mu\text{m}$  mesh porous silica particles in pure nitrobenzene.

The dielectric constant is a natural choice of order parameter to study freezing of dipolar liquids because of the large change in the orientational polarizability between the liquid and solid phases. The melting point was taken to be the temperature at which there was a large increase in the permittivity as the solid phase was heated. The frequency range chosen for measurements corresponds to the typical dielectric relaxation times in the solid phase. The dielectric relaxation time was calculated by fitting the dispersion spectrum of the complex permittivity near resonance to the Debye model of orientational relaxation. The modified Debye dispersion relation is given by<sup>22,23</sup>

$$\kappa^* - \kappa'_\infty = \frac{\kappa'_s - \kappa'_\infty}{1 + (\omega\tau)^{1-h}} \quad (4)$$

where  $\omega$  is the frequency of the applied potential and  $\tau$  is the orientational (rotational) relaxation time of a dipolar molecule. The subscript  $s$  refers to static permittivity (low frequency limit, when the dipoles have sufficient time to be in phase with the applied field). The subscript  $\infty$  refers to the optical permittivity (high-frequency limit) and is a measure of the induced component of the permittivity. In eq 4,  $h$  is an empirical parameter that has a value between 0 and 1 and is a measure of the deviation from the original Debye equation (for which  $h = 0$ ).

**2.3. Computer Simulation.** We study the freezing of Lennard-Jones (LJ) methane in slit-shaped pores. We consider two kinds of pore wall interactions: a hard wall, which corresponds to a purely repulsive fluid–wall interaction, and a graphite wall, for which the fluid–wall interaction is strongly attractive. Since our main focus was on the calculation of the free energy, we chose a simpler (slit-shaped) geometry that models carbon (graphite) pores. The simulation runs were all performed in the grand canonical ensemble as described in ref 24, fixing the chemical potential  $\mu$ , the volume  $V$  of the pore, and the temperature  $T$ . The pore width  $H$  in the simulation was typically around  $7.5\sigma_{\text{ff}}$ , and the rectilinear simulation cell was  $10\sigma_{\text{ff}}$  by  $10\sigma_{\text{ff}}$  in the plane parallel to the pore walls, consistent with a potential cutoff of  $5\sigma_{\text{ff}}$  for the fluid–fluid interaction. The system typically contained up to 700 particles, and periodic boundary conditions were employed in the plane parallel to the pore walls. Thermodynamic properties were averaged over 40–100 million individual Monte Carlo steps.

To model the graphite pore, we use the integrated 10–4–3 Steele potential<sup>25,26</sup> given by

$$\phi_{\text{fw}}(z) = 2\pi\rho_w\epsilon_{\text{fw}}\sigma_{\text{fw}}^2\Delta\left[\frac{2}{5}\left(\frac{\sigma_{\text{fw}}}{z}\right)^{10} - \left(\frac{\sigma_{\text{fw}}}{z}\right)^4 - \left(\frac{\sigma_{\text{fw}}^4}{3\Delta(z + 0.61\Delta)^3}\right)\right] \quad (5)$$

The potential parameters for LJ methane and for the graphite wall were taken from Steele:<sup>25,26</sup>

$$\sigma_{\text{ff}} = 0.381 \text{ nm}, \quad \epsilon_{\text{ff}}/k_B = 148.1 \text{ K}$$

$$\sigma_{\text{ww}} = 0.340 \text{ nm}, \quad \epsilon_{\text{ww}}/k_B = 28.0 \text{ K}$$

$$\rho_w = 114 \text{ nm}^{-3}, \quad \Delta = 0.335 \text{ nm}$$

$$\sigma_{\text{fw}} = (\sigma_{\text{ff}} + \sigma_{\text{ww}})/2, \quad \epsilon_{\text{fw}} = (\epsilon_{\text{ff}}\epsilon_{\text{ww}})^{1/2}$$

The subscripts  $f$  and  $w$  denote fluid and wall, respectively, and  $z$  is the coordinate perpendicular to the pore walls. For a given pore width  $H$ , the total potential energy from both walls is given by

$$\phi_{\text{pore}}(z) = \phi_{\text{fw}}(z) + \phi_{\text{fw}}(H - z) \quad (6)$$

Here  $H$  is defined to be the distance between the planes through the carbon nuclei in the first atomic layer of each of the opposing walls.

The standard method to calculate the free energies of solid and fluid phases is thermodynamic integration.<sup>27</sup> This method involves a numerical integration of the Gibbs free energy, starting from a known reference phase (the Einstein crystal for the solid phase and the ideal gas for the liquid phase) to the state point of interest. It relies on finding a suitable path of integration which is thermodynamically reversible; i.e., the path does not intersect any phase boundary characterized by a first-order transition. Dominguez et al.<sup>20</sup> employed this method to calculate the Gibbs free energy for an LJ fluid in purely repulsive and weakly attractive slit pores. They found the location of the thermodynamic transition temperature and also showed that the transition was first order.

For the more ubiquitous case of a wall–fluid potential that is moderately or strongly attractive, the method of thermodynamic integration breaks down. This is because the adsorbed molecules adjacent to the pore wall (the contact layer) freeze before the molecules in the interior of the pore. This makes it impossible to find a reversible path from the ideal gas phase to the fluid phase, since any such path runs into a first-order transition corresponding to the freezing of the contact layer. To overcome this difficulty, we use a method based on an order parameter formulation to calculate the free energy; this approach was first used to study solid–fluid transitions in the bulk by Van Duijneveldt et al.<sup>28,29</sup> The method relies on the calculation of the Landau free energy as a function of an effective bond orientational order parameter  $\Phi$ , using GCMC simulations. The Landau free energy is defined by<sup>30</sup>

$$\Delta[\Phi] = -k_B T \ln(P[\Phi]) + \text{constant} \quad (7)$$

where  $P[\Phi]$  is the probability of observing the system having an order parameter value between  $\Phi$  and  $\Phi + \delta\Phi$ . The probability distribution function  $P[\Phi]$  is calculated in a GCMC simulation by collecting statistics of the number of occurrences of a particular value of  $\Phi$  in the form of a histogram, with the help of umbrella sampling.<sup>31</sup> The grand free energy  $\Omega$  is then related to the Landau free energy by

$$\exp(-\beta\Omega) = \int d\Phi \exp(-\beta\Delta[\Phi]) \quad (8)$$

The grand free energy at a particular temperature can be calculated by numerically integrating eq 8 over the order parameter space. More complete details of the method for confined systems are given elsewhere.<sup>32</sup>

(22) Debye, P. *Polar Molecules*; Chemical Catalog Co.: New York, 1929.

(23) Cole, K. S.; Cole, R. H. *J. Chem. Phys.* 1941, 9, 341.

(24) Woods, G. B.; Rowlinson, J. S. *J. Chem. Soc., Faraday Trans 2* 1989, 85, 765.

(25) Steele, W. A. *Surf. Sci.* 1973, 36, 317.

(26) Steele, W. A. *The interaction of gases with solid surfaces*; Pergamon Press: Oxford, U.K., 1974.

(27) Frenkel, D.; Ladd, A. J. C. *J. Chem. Phys.* 1984, 81, 3188.

(28) Van Duijneveldt, J. S.; Frenkel, D. *J. Chem. Phys.* 1992, 96, 4655.

(29) Lynden-Bell, R. M.; Van Duijneveldt, J. S.; Frenkel, D. *Mol. Phys.* 1993, 80, 801.

(30) Landau, L. D.; Lifshitz, E. M. *Statistical Physics*, 3rd ed.; Pergamon Press: London, 1980.

(31) Torrie, G. M.; Valleau, J. P. *Chem. Phys. Lett.* 1974, 28, 578.

(32) Radhakrishnan, R.; Gubbins, K. E. *Mol. Phys.*, in press.

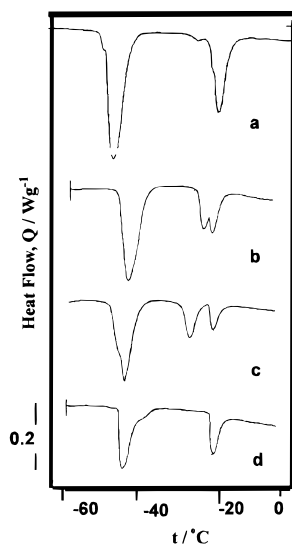


Figure 1. Representative DSC scans for melting of  $\text{CCl}_4$  in CPG, after subtraction of the background signal. Results are for mean pore sizes of (a) 100 nm (the second minimum occurs as a shoulder in the main peak at  $-21.2$  °C), (b) 40 nm, (c) 20 nm, and (d) 7.5 nm (the second minimum occurs as a shoulder in the solid–solid peak at  $-44.0$  °C). Each scan is shifted in the vertical scale for the sake of clarity.

### 3. Experimental Results

**3.1. Differential Scanning Calorimetry (DSC).** In Figure 1 is shown the evolution in the DSC patterns of several different  $\text{CCl}_4$ –CPG samples obtained during melting runs. The results were found to be independent of the heating rate in the range  $0.5$ – $5$  °C/min. The relatively large minimum at  $-21.2$  °C that is independent of pore size corresponds to the melting of the bulk  $\text{CCl}_4$  in which the porous particles are suspended. In addition, a second minimum that is dependent on the pore size is also observed. This signal corresponds to the melting of the  $\text{CCl}_4$  in the pores and shifts to lower temperatures as the pore size is reduced. The third minimum (at  $t = -44$  °C) that is also independent of pore width corresponds to a solid–solid phase transition (monoclinic to rhombohedral structure at  $-46$  °C<sup>33</sup>) in the bulk  $\text{CCl}_4$ . In some cases (Figure 1a,c) a fourth minimum occurs that may be due to such a solid–solid transition in the pore (this peak is seen as a shoulder in the solid–solid peak below  $t = -44$  °C); however, DSC results alone are inconclusive in this regard. The size dependence of the melting temperature of the confined  $\text{CCl}_4$  is shown in Figure 2. The linear relationship between the shift in the pore melting temperature and the inverse pore diameter is consistent with the Gibbs–Thomson equation down to the smallest pore size studied ( $H = 7.5$  nm). A direct test would however involve the independent measurement of the wall–fluid and the wall–solid interfacial tensions, which we have not attempted.

DSC scans corresponding to melting of nitrobenzene are shown in Figure 3. The qualitative behavior is the same as in the case of  $\text{CCl}_4$ . The melting point of the bulk is  $-5.6$  °C (monoclinic crystal phase to liquid<sup>34</sup>). The melting point in the pore is always depressed, and the magnitude of the shift increases with decreasing pore size.

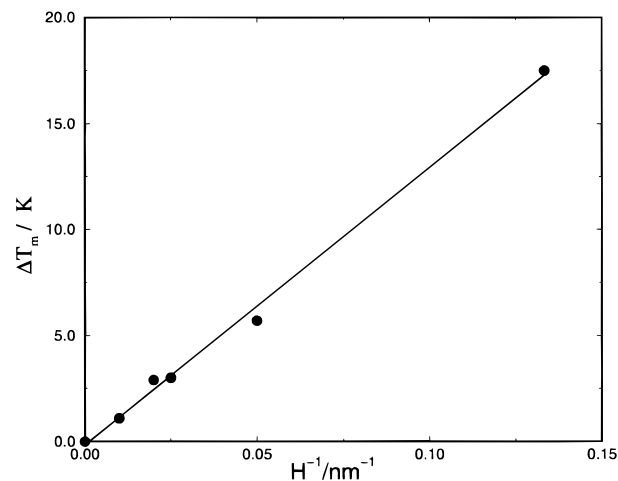


Figure 2. Shift in the melting temperature  $\Delta T_m = T_{m,\text{bulk}} - T_{m,\text{pore}}$  as a function of  $1/H$  for  $\text{CCl}_4$  in CPG. The straight-line fit is consistent with the Gibbs–Thomson equation, which is valid in the large-pore limit.

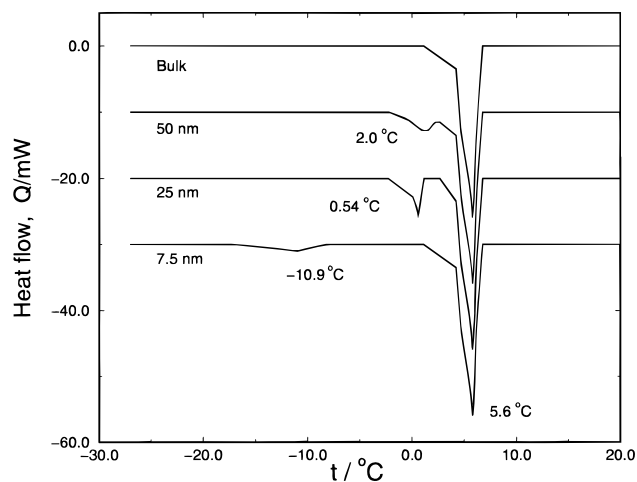


Figure 3. Representative DSC scans for melting of nitrobenzene in CPG, after subtraction of the background signal. Each scan is shifted in the vertical scale for the sake of clarity.

Table 1. Heats of Melting for Nitrobenzene

pore size, $H$ (nm)	latent heat, $\lambda_m$ (J/g)	$t_m$ (°C)
bulk	94.5	5.6
50	79.5	3.4
25	50.0	0.4
7.5	43.8	-16.0

As the pore size becomes smaller, the pore melting peak broadens and becomes increasingly asymmetric. Since the signals corresponding to the confined nitrobenzene are better resolved and separated from the bulk signal than for the case of  $\text{CCl}_4$ , we have calculated the latent heat of melting for the bulk and confined solids. The amounts of nitrobenzene partitioned between the bulk and the pore were determined by requiring the bulk signal to give the correct bulk latent heat. The values of the melting temperature  $t_m$  and the latent heat of melting  $\lambda_m$  are summarized in Table 1. One possible explanation of the decrease in the latent heat values with decreasing pore size is that the crystal structure of the confined solid phase becomes increasingly disorganized as the pore size decreases.

**3.2. Dielectric Spectroscopy.** The capacitance  $C$  and tangent loss  $\tan(\delta)$  were measured as a function of frequency and temperature for bulk nitrobenzene and for

(33) Parsonage, N. G.; Staveley, L. A. K. *Disorder in Crystals*; International Series of Monographs in Chemistry; Clarendon Press: Oxford, U.K., 1978.

(34) Donnay, J. D. H.; Ondik, H. M. *Crystal Data Determinative Tables*, 3rd ed.; National Bureau of Standards: Washington, DC, 1978; Vol. 1.

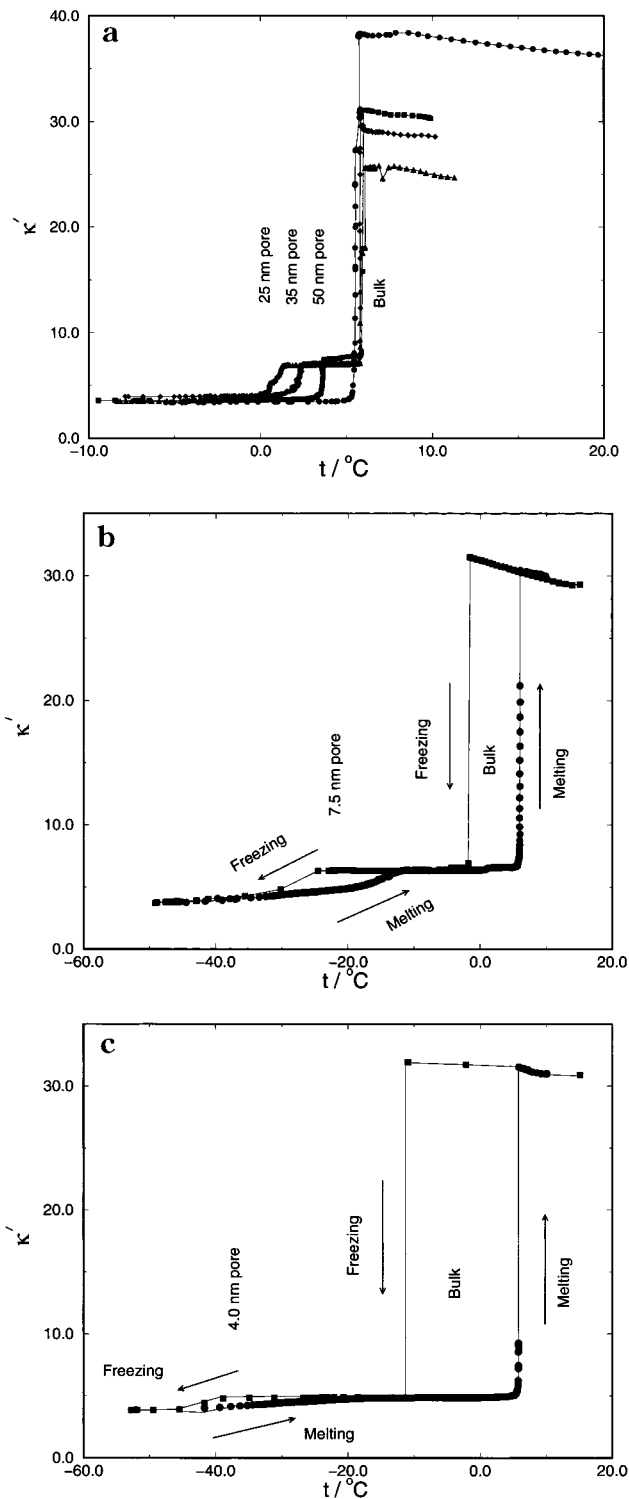


Figure 4. Relative permittivity,  $\kappa'$ , as a function of temperature for different pore widths: (a) equilibrium measurements during melting process; (b, c) measurements showing melting and freezing along with the hysteresis for smaller pores. The measured permittivity is an effective value for the suspension of the porous silica glass in pure nitrobenzene.

nitrobenzene adsorbed in CPG and Vycor glass of different pore sizes ranging from 50 to 4.0 nm. The behavior of  $\kappa'$  vs  $T$  is shown in Figure 4 for nitrobenzene in pores of different widths, calculated at a typical frequency of 1 MHz using eq 3. For pure, bulk nitrobenzene, there is a sharp increase in  $\epsilon'$  at  $t = 5.6$  °C, corresponding to the melting point of the pure substance. For nitrobenzene confined in CPG, the sample is introduced as a suspension

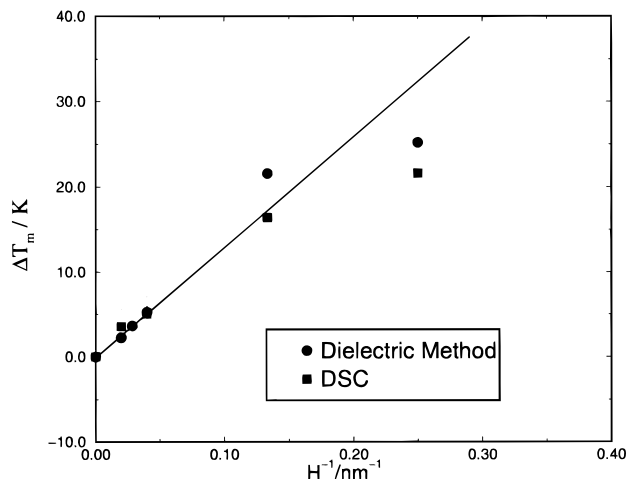


Figure 5. Shift in the melting temperature  $\Delta T_m = T_{m,bulk} - T_{m,pore}$  as a function of  $1/H$  for nitrobenzene in CPG. The DSC and the DS measurements are in good agreement. The straight line is a fit to the data for  $H$  values of 7.5 nm and above and is consistent with the Gibbs–Thomson equation.

of nitrobenzene-filled CPG particles in pure nitrobenzene, between the capacitor plates. Thus capacitance measurement yields an effective relative permittivity of the suspension of CPG in pure nitrobenzene. And thus  $\kappa'$  shows two sudden changes. The increase that depends on pore size is attributed to melting in the pores, while that at 5.6 °C corresponds to the bulk melting. It is interesting to note that the signal corresponding to the melting in pores becomes increasingly rounded as the pore size becomes smaller, in much the same way as the broadening of the peaks in DSC. For smaller pore sizes ( $H = 7.5$  and 4.0 nm), the increase in  $\kappa'$  is continuous. Both the melting and freezing signals are shown; the hysteresis loops grow wider with decreasing pore size. The rounding of the increase in  $\kappa'$  is expected to be smaller than the width of the peaks in the DSC scans, as the capacitance is measured at equilibrium. The shifts in the melting temperature are plotted against the reciprocal pore width in Figure 5 for nitrobenzene in CPG obtained using both DSC and DS measurements. The deviations from linearity, and hence from the Gibbs–Thomson equation, are appreciable at pore widths as small as 4.0 nm.

The spectrum of the complex permittivity ( $\kappa'$ ,  $\kappa''$  vs  $\omega$ ) is fit to the dispersion relation (eq 4) to determine the dielectric relaxation time  $\tau$ , which gives valuable information about the structure of the condensed phase. The frequency range in this study is expected to encompass the resonant frequencies corresponding to the dielectric relaxation in the solid phases. To probe the liquid relaxation behavior would require a frequency range that is 4–5 orders of magnitude higher. The modified Debye dispersion relation can be expressed in normalized form<sup>35</sup> as

$$\frac{\kappa' - \kappa'_\infty}{\kappa'_s - \kappa'_\infty} = \frac{1}{2} \left( 1 - \frac{\sinh(z)}{\cosh(z) + \sin(h\pi/2)} \right) \quad (9)$$

$$\frac{\kappa''}{\kappa'_s - \kappa'_\infty} = \frac{1}{2} \left( \frac{\cos(h\pi/2)}{\cosh(z) + \sin(h\pi/2)} \right) \quad (10)$$

where the normalized variable  $z$  is given by  $z = (1 - h) \times \ln(\omega\tau)$ . According to eqs 9 and 10, the  $\kappa'$  function shows a point of inflection and the  $\kappa''$  function goes through a

(35) Frölich, H. Theory of Dielectrics; Clarendon Press: Oxford, U.K., 1949; p 73.

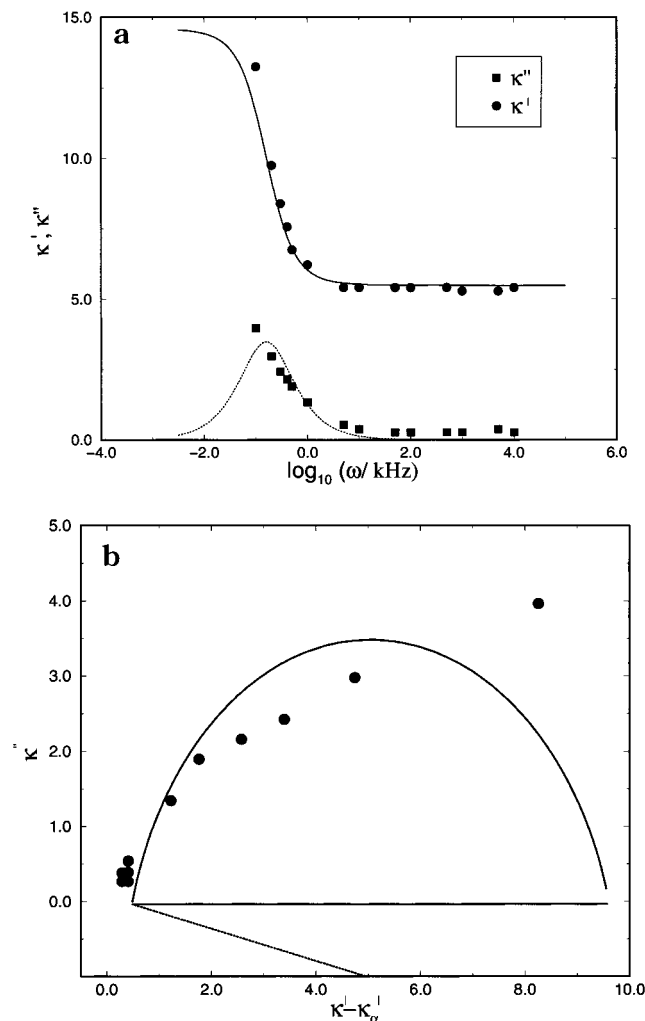


Figure 6. (a) Spectrum plot for nitrobenzene in a 7.5 nm pore at  $t = -21$  °C. The solid and the dashed curves are fits to eqs 9 and 10, respectively. (b) The same parameters in the Cole–Cole representation.

maximum at  $z = 0$ . Therefore, from a spectrum plot of  $\kappa'$ ,  $\kappa''$  vs  $\log(\omega)$ , the relaxation time can be calculated as the reciprocal of the frequency corresponding to a saddle point of the  $\kappa'$  function or a maximum of the  $\kappa''$  function. An alternative graphical representation of the modified Debye dispersion equation can be obtained through a Cole–Cole plot<sup>23</sup> in the complex  $\kappa^*$  plane. From a plot of  $\kappa''$  vs  $\kappa'$ ,  $\tau$  is given by the reciprocal of the frequency at which  $\kappa''$  goes through a maximum.

The spectrum plot and Cole–Cole plot for nitrobenzene in a 7.5 nm CPG at  $t = -21$  °C are shown in Figure 6. The solid and dashed curves fit the experimental data points accurately, indicating a Debye type relaxation with a single time scale. The relaxation time is estimated to be  $\tau = 1.44$  ms. At a different temperature ( $t = -4$  °C), the behavior is significantly different (Figure 7). The double-peak structure of the  $\kappa''(\omega)$  curve and the double inflection in the  $\kappa'(\omega)$  curve suggest two different dielectric relaxation times. The Cole–Cole plot for such a behavior<sup>36</sup> falls on two semicircles. There is a shorter relaxation time  $\tau_1 = 43.6$   $\mu$ s, in addition to the longer components  $\tau_2 = 1.7$  ms.

#### 4. Simulation Results

4.1. Hard-Wall Pore. The adsorption curve (Figure 8) and the pair correlation  $\kappa$  functions were calculated for

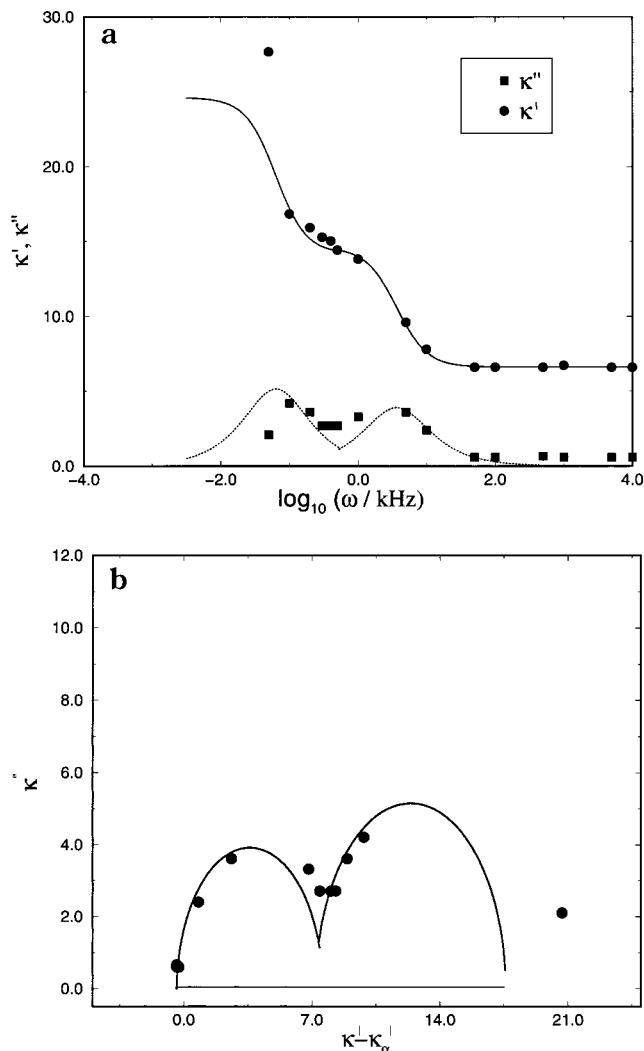


Figure 7. (a) Spectrum plot for nitrobenzene in a 7.5 nm pore at  $t = -4$  °C. The solid and the dashed curves are fits to eqs 9 and 10, respectively. (b) The same parameters in the Cole–Cole representation. This plot yields two distinct Debye relaxation times.

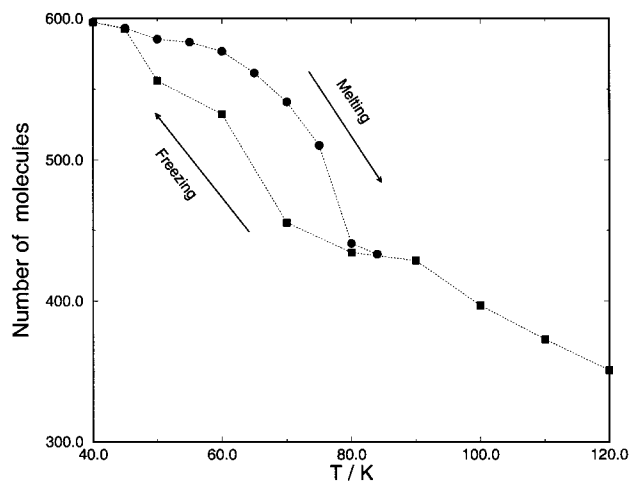


Figure 8. Variation of adsorption with temperature, at a fixed bulk-phase pressure of 100 atm, for LJ methane confined in the hard-wall pore of width  $H = 7.5 \sigma_{\text{ff}}$ . The freezing occurs at  $T \approx 40$  K, and melting occurs at  $T \approx 80$  K. Thus, a pronounced hysteresis loop occurs, spanning about 40 K.

methane confined in a hard-wall slit pore of width  $7.5 \sigma_{\text{ff}}$  using standard GCMC simulations. The chemical potential

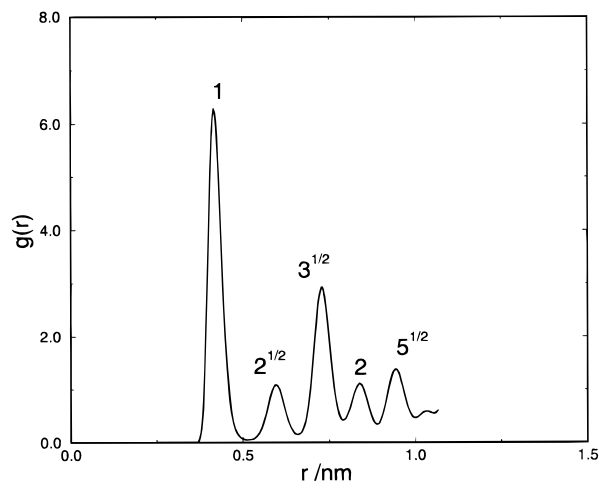


Figure 9. Pair correlation function of the solid phase of methane confined between hard walls at  $T = 45$  K and  $P = 100$  atm. This correlation function is equivalent to a powder diffraction pattern in real space. From the positions of the first five peaks in the pair correlation function (at  $r/\sigma_{\text{ff}} = 1, 2^{1/2}, 3^{1/2}, 2,$  and  $5^{1/2}$ ), it is evident that the crystal structure could be either a simple cubic lattice or a face-centered-cubic lattice.

was maintained at a value corresponding to a bulk pressure of 100 atm at all temperatures; the LJ equation of state<sup>37</sup> was used to relate the chemical potential to the pressure. This high pressure is necessary to study hard-wall systems because the methane would evaporate inside such pores under normal pressures.<sup>18</sup> These results suggested that the structures of the fluid and solid phases are similar to the bulk three-dimensional structure, but the transition occurs at a much lower temperature than for bulk methane; the freezing point of Lennard-Jones methane in the bulk is  $T = 101$  K.<sup>38,39</sup> Three-dimensional bond orientational order parameters introduced by Steinhardt et al.<sup>40</sup> were employed for the calculation of the grand free energy. From the positions of the first five peaks in the pair correlation function of the solid phase (Figure 9), it is evident that the crystal structure could be either a simple cubic lattice or a face-centered-cubic lattice. The calculation of the order parameters confirmed that the crystal structure is face-centered cubic.

The Landau free energy (LFE) as a function of the order parameter has a characteristic double-well structure with a broad minimum centered around the order parameter  $\Phi = 0$ , corresponding to the liquid phase, and a second minimum centered around  $\Phi = 0.95$ , corresponding to the face-centered-cubic phase ( $\Phi_{\text{fcc}} = 1.052$  for an ideal crystal) for two different temperatures,  $T = 60$  K and  $T = 45$  K. The high-temperature LFE curve showed the liquid phase to be more stable, while the low-temperature curve showed the crystal phase to be the most stable. The grand free energy for each phase is calculated from the Landau free energy using eq 8 and is shown in Figure 10. The crossover of the liquid and solid branches at different slopes clearly establishes the transition as first order and also determines the transition point at  $T = 48$  K, which should be compared to the bulk transition of  $T = 101$  K for LJ methane.

4.2. Graphite Pore. The adsorption curve for methane adsorbed in the graphite pore was calculated along a path

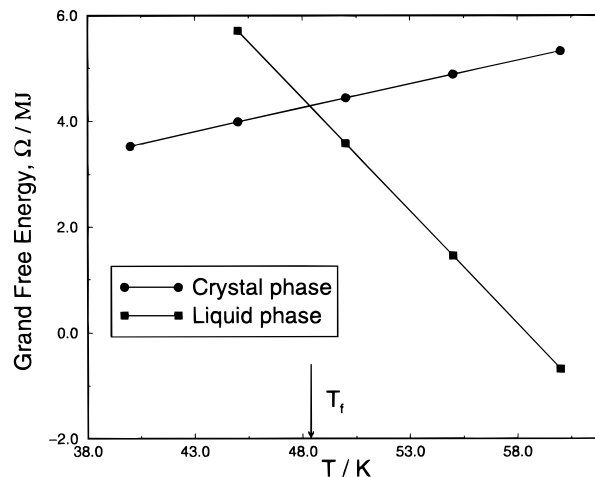


Figure 10. Grand free energy  $\Omega$  of the liquid and the crystal phases as a function of temperature for the hard-wall system. The crossover point near  $T = 48$  K determines the thermodynamic transition temperature.

such that, for each temperature, the value of the chemical potential corresponds to the pressure at which there is two-phase (gas–liquid for temperatures above the triple point and gas–solid below the triple point) coexistence in the bulk fluid.<sup>38,39</sup> This path was chosen so that our calculations could be verified in a real experiment, without having to depend on an accurate LJ equation of state.<sup>18</sup> The adsorption behavior for methane in graphite for two slightly different pore widths is shown in Figure 11. Both systems have seven molecular layers of methane, yet the extent of hysteresis is much larger for the slightly smaller pore. The density profile along the  $z$  direction (the direction perpendicular to the pore walls) is shown in Figure 12. In contrast to the behavior for a hard wall, distinct layering occurs for the whole range of temperatures for which freezing and melting occur. To incorporate this feature, we choose a two-dimensional order parameter previously introduced by Mermin<sup>41</sup>

$$\Phi_j = \left| \frac{1}{N_{b,k=1}} \sum_{k=1}^{N_b} \exp(i6\theta_k) \right| \equiv |\langle \exp(i6\theta_k) \rangle_j| \quad (11)$$

where  $N_b$  is the number of bonds in layer  $j$  and  $\Phi_j$  measures the average hexagonal bond order within each layer  $j$ . The overall order parameter  $\Phi$  is an average of the hexagonal order in all the layers:

$$\Phi = \left( \sum_{j=1}^{N_{\text{layers}}} \Phi_j \right) / N_{\text{layers}} \quad (12)$$

Unlike the hard-wall confinement case (or the bulk behavior), this system is characterized by three phases A, B, and C, indicated by the presence of three different minima in the LFE curves (Figure 13a). The structures of the three phases are shown in Figure 13b–d. In phase A, all the layers have an isotropic liquid-like structure; phase B is characterized by frozen contact layers, with the rest of the layers having a liquid-like structure; and in phase C, all the layers are frozen. The LFE results clearly indicate that the contact layers (layers adjacent to the pore walls) freeze at a higher temperature compared to the inner layers. The freezing point of the contact layers and that of the inner layers were determined exactly by

(37) Johnson, J. K.; Zollweg, J. A.; Gubbins, K. E. *Mol. Phys.* 1993, 78, 591.

(38) Kofke, D. A. *J. Chem. Phys.* 1993, 98, 4149.

(39) Agrawal, R.; Kofke, D. A. *Mol. Phys.* 1995, 85, 43.

(40) Steinhardt, P. J.; Nelson, D. R.; Ronchetti, M. *Phys. Rev. B* 1983, 28, 784.

(41) Mermin, N. D. *Phys. Rev.* 1968, 176, 250.

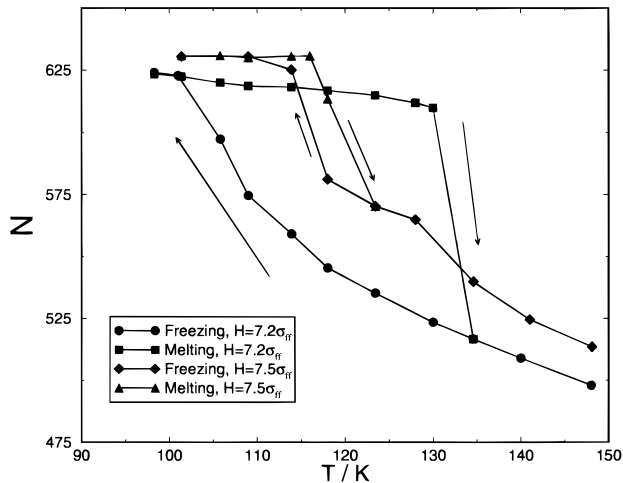


Figure 11. Freezing and melting curves, showing the number of molecules adsorbed in the system as a function of temperature for two pore widths,  $H = 7.5\sigma_{ff}$  and  $H = 7.2\sigma_{ff}$ .  $N$  is the average number of molecules in the system. A slight change in the pore width causes a large change in the hysteresis behavior. The adsorption and desorption paths are along the two-phase (gas–liquid for temperatures above the triple point and gas–solid below the triple point) coexistence line for the bulk.

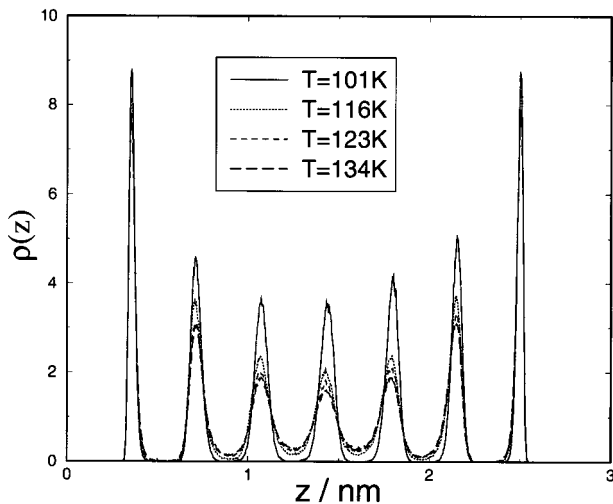


Figure 12. Density profiles of methane in the graphite pore along the direction perpendicular to the pore walls for four different temperatures, showing distinct layering. Here,  $\rho(z)$  is expressed as number of molecules per unit length along the  $z$  axis. The solid curve for  $T = 101$  K is for the crystalline methane and is not quite symmetric about the center of the pore along the  $z$  axis because of defects in the two-dimensional crystal phase in the second and third layers. The profiles for the other temperatures correspond to a fluid phase and possess the symmetry.

calculating the grand free energy. This calculation is depicted in Figure 14 for the three phases A, B, and C. The plot indicates two first-order transitions, one at  $T = 124$  K, corresponding to the freezing of the contact layers, and the other at  $T = 114$  K, corresponding to the freezing point in the inner layers.

## 5. Discussion and Conclusions

The simulation results and the Gibbs–Thomson equation suggest that the fluid–wall interaction for  $\text{CCl}_4$  and nitrobenzene in CPG is less than the respective fluid–fluid interaction, and thus the freezing temperature is always depressed. For  $\text{CCl}_4$  in CPG, this is a reasonable scenario if we realize that the fluid–wall potential energy

is proportional to  $\rho_w \epsilon_{fw}$  ( $\rho_w$  being the density of substrate atoms in the pore and  $\epsilon_{fw}$  being the fluid–wall energy parameter if we assume an LJ potential). The ratio of the fluid–wall potential energy to the potential energy that would exist if the wall was composed of the fluid molecules is then  $\rho_w \epsilon_{fw} / \rho_s \epsilon_{ff}$ . This ratio is about 0.5 for  $\text{CCl}_4$  in CPG. A more accurate estimate would involve the LJ size parameter  $\sigma_{fw}$  and a geometrical factor that depends on  $H/\sigma_{fw}$ ,  $H$  being the pore diameter. For nitrobenzene in CPG, the situation is further complicated by the longer range dipolar interaction, which introduces a term in addition to the LJ interaction.

The permittivity measurements (the behavior of  $k'$  with  $T$ ) show that the melting transition in larger pores ( $H \geq 25$  nm) is abrupt (e.g., Figure 4a) and becomes increasingly rounded in smaller pores ( $H = 7.5$  and  $4.0$  nm), where it appears continuous (e.g., Figure 4b,c). This behavior in smaller pores is also seen in simulations and is apparent if we compare the general trends in Figure 11 and Figure 15. The free energy calculation clearly shows that the freezing in such narrow pores is also first order. The presence of a discontinuity in the slope of the free energy curve at the transition point is a measure of the first-order jump in the heat capacity. Thus, in these simulations, the hysteresis loops in the behavior of the density as a function of temperature are due to the existence of metastable states. Radhakrishnan and Gubbins<sup>32</sup> have studied the origin of these metastable states for methane confined in graphitic carbon. In a real experiment, however, slow diffusion and pore blocking can also contribute to the hysteresis behavior.

The typical dielectric relaxation time for a dipolar liquid in the bulk phase is  $10^{-9}$  s. The relaxation time increases in  $10^{-3}$  s when the liquid freezes to a crystal phase.<sup>21</sup> For dipolar molecules confined in nanoscale silica pores, the typical liquid-phase relaxation time is slightly higher compared to that of the bulk phase and is about  $10^{-8}$  s.<sup>42,43</sup> In addition, for a heterogeneous system, there occurs a relaxation mechanism due to interfacial polarization when a slightly conducting liquid is enclosed in an insulating material. This effect, also called the Maxwell–Wagner–Sillars (MWS) polarization,<sup>44</sup> is known to have a relaxation time of the order of  $10^{-3}$  s.<sup>43,45</sup> The CPG and Vycor samples used in this study were dielectrically neutral, in the sense that, in the temperature and frequency ranges of our measurements, the dielectric losses (proportional to  $\kappa''$ ) of the empty pores were negligible compared to those of the liquid-filled samples. Therefore, there is no background noise due to the motion of silica molecules. The dielectric relaxation component for nitrobenzene in CPG at  $t = -22$  °C, with a relaxation time  $\tau = 1.44$  ms (Figure 6), is attributed to the crystalline solid phases in the bulk and the pore. At  $t = -4$  °C, the bulk phase is still a crystalline solid, while the confined phase is a liquid. In this case (Figure 7), two distinct relaxation times appear, corresponding to two different relaxation mechanisms. The longer component relaxation,  $\tau_2 = 1.7$  ms, is attributed to the bulk crystalline phase of nitrobenzene. The shorter relaxation component,  $\tau_1 = 43.6$   $\mu$ s, is too slow to represent the liquid-phase relaxation in the pore. However, it is known that, for dipolar liquids confined in nanoscale pores, the molecules in the contact layer show a slower relaxation

(42) Schüller, J.; Mel'nichenko, Yu. B.; Richert, R.; Fischer, E. W. *Phys. Rev. Lett.* 1994, 73, 2224.

(43) Pissis, P.; Kyritsis, A.; Daoukaki, D.; Barut, B.; Pelster, R.; Nimtz, G. *J. Phys. Condens. Matter* 1998, 10, 6205.

(44) Bánhegyi, G. *J. Colloid Polym. Sci.* 1986, 264, 1030.

(45) Schüller, J.; Richert, R.; Fischer, E. W. *Phys. Rev. B* 1995, 52, 15232.

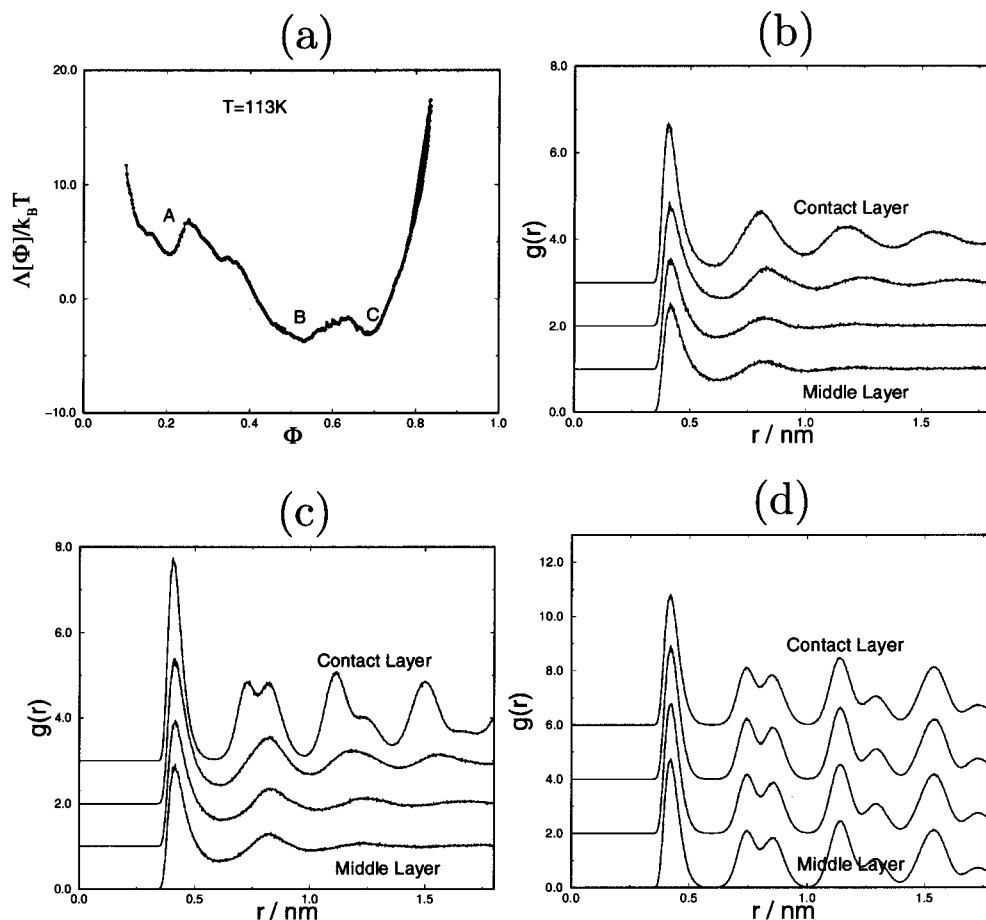


Figure 13. (a) Landau free energy at 113 K as a function of the order parameter, for LJ methane confined in a graphite pore of width  $7.5\sigma_{ff}$  showing three different phases. The stable phase at this temperature is B. (b–d) Two-dimensional, in-plane pair correlation functions for each of the layers for the  $H = 7.5\sigma_{ff}$  graphite pore: (b)  $T = 130$  K, corresponding to phase A; (c)  $T = 123$  K, corresponding to phase B; (d)  $T = 101$  K, corresponding to phase C. Only four of the seven layers are shown because of the symmetry about the midplane.

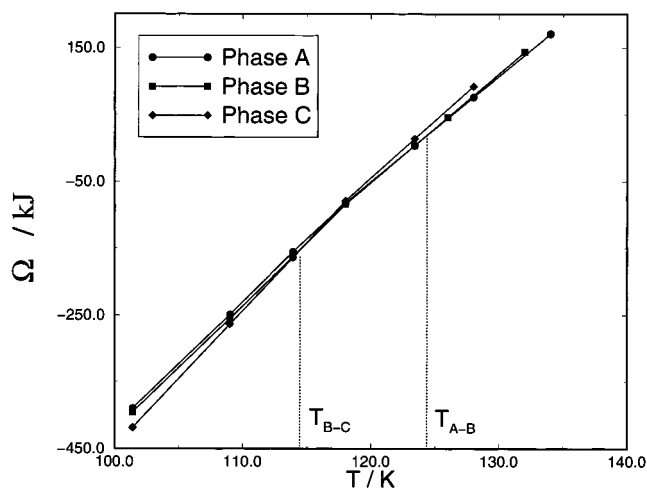


Figure 14. Grand free energy  $\Omega$  of the three phases A, B, and C, as a function of temperature for LJ methane in the graphite pore. The crossover points  $T_{A-B}$  and  $T_{B-C}$  correspond to the two first-order phase transitions.

behavior, on the order of  $10^{-6}$  s.<sup>43,45,46</sup> Thus, the shorter relaxation component is consistent with such a behavior of the contact layer. The Landau free energy calculation for methane in graphite and the NMR study by Overloop and Van Gerven<sup>14</sup> dealing with water in porous silica also

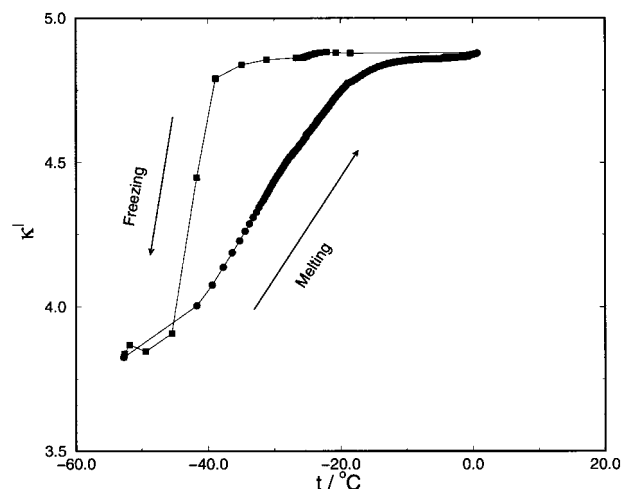


Figure 15. Hysteresis associated with melting and freezing of nitrobenzene in a 7.5 nm CPG obtained using dielectric spectroscopy measurements.

support the view that the molecules in the contact layer behave differently from the those in the pore interior.

We also observed two relaxation mechanisms for temperatures greater than  $t = 5.6$  °C, one corresponding to the relaxation of the molecules in the contact layer in the pores and the other (in the range of  $10^{-3}$  s) arising because of MWS polarization. We note that, in this study, we were unable to resolve the MWS relaxation component

from the crystalline phase relaxation. We propose to carry out extensive dielectric spectroscopy measurements for different pore sizes, for a larger range of frequencies (to probe the liquid-phase relaxation behavior), and for varying amounts of nitrobenzene to realize different degrees of pore filling. Such a study is expected to differentiate between the MWS relaxation and the solid-phase relaxation. We also plan to use NMR measurements and to compare these with the dielectric spectroscopy results.

Our experimental system was limited to porous silica glasses in this study. We plan to study other porous systems that have a strongly attractive fluid-wall potential, such as well-characterized carbons. It would be interesting to see if there is an increase in freezing temperature of simple fluids in such attractive pores, as predicted by the simulation results and the Gibbs-Thomson equation. The simulation results for methane in graphite are consistent with the observed increase of the freezing temperature in experimental studies of methane adsorbed on a single graphite substrate by Castro et al.<sup>47</sup> Recently, Kaneko<sup>48</sup> reported a large increase in freezing temperature of  $\text{CCl}_4$  in slitlike graphite pores. We are currently studying this system by computer simulation to compare with the experimental results. We

---

(47) Castro, M. A.; Clarke, S. M.; Inaba, A.; Thomas, R. K. *J. Phys. Chem. B* 1997, 101, 8878.

(48) Kaneko, K. Private communication, 1998.

plan to use the Landau free energy method to investigate the freezing behavior.

Efforts are underway to use more realistic fluid potentials and pore models in the simulation. Recently Gelb and Gubbins<sup>49</sup> proposed a novel mechanism to realistically model porous silica glasses using spinodal decomposition of a binary fluid mixture in the two-phase liquid-liquid region. This model is known to closely represent the actual pore size distribution of real porous silica and incorporates complex pore networking. We plan to study freezing of simple fluids using the free energy method in such a pore model and to directly compare to these experimental results for  $\text{CCl}_4$  in CPG.

**Acknowledgment.** It is a pleasure to thank K. Kaneko and M. Miyahara for helpful discussions. R.R. thanks Adama Mickiewicz University, Poznan, Poland, for hospitality during a visit in the summer of 1998, when this work was carried out. This work was supported by grants from the National Science Foundation (CTS-9896195) and KBN (2 PO3B 175 08) and by a grant from the U.S.-Poland Maria Sklodowska-Curie Joint Fund (MEN/DOE-97-314). Supercomputer time was provided by an NSF/NRAC grant (MCA93S011).

LA9814642

---

(49) Gelb, L. D.; Gubbins, K. E. *Langmuir* 1998, 14, 2097.